International Journal of Science and Research (IJSR)
ISSN: 2319-7064
Impact Factor 2024: 7.101

Nanophase-Prepared Undoped Magnetic Stannic Dioxide Semiconductor for Space Applications

Sanjoo Yadav[1], Anant Kumar[2], Ashok Kumar[3]

Department of Physics, HD Jain College, VKS University, Ara
Physics Department, RamRatan Singh College, Mokama, PPU, Patna

Abstract: ***Nanophase materials have emerged instrumental in space science applications. Among them, stannic dioxide nanoparticles are especially focused due to their wide band gap, large surface-to-volume ratio, gas sensing, high chemical stability, thermal absorptivity, energy and photocatalytic actions. In spacecrafts, it serves in atmosphere monitoring and purification of air and water, and biosensor of gas like methane and coupled to cryogenic or volcanic plume analyzers on moons. Here we report ecofriendly synthesis of nanophase stannic dioxide and its features based on x-ray diffraction, WH plot, and zeta potential (stability) measurements. Unit cells are found tetragonal with lattice parameters a and b, equal to 4.75 Å each, and c=3.22 Å. Williamson-Hall plot gives a particle size of 3.13 nm with a positive micro-strain of 0.012. Stability and agglomeration suggested by the observed values of zeta potentials are consistent with SEM image. It exhibits blue shifted band gap of 4.39 eV, measured from Tauc's plot in uv-visible range, suitable for photocatalysis and energy applications in space. Using VSM measurement, hysteresis was observed in M-H plane which indicated to ferromagnetism in pure SnO_2 without any magnetic element doping, possibly attributable to defect states.***

Keywords: Space science, zeta potential, stannic dioxide nanoparticle, WH plot, stability, spacecraft, ferromagnetism

1. Introduction

Space science material research has recently incorporated nanophase materials. The most interesting section of space science for nanomaterials arises because of availability of engineered materials of high sensitivity, light weight, radiation resistance, transparency and stability in extreme conditions of temperature and pressure. Areas like detection of trace gases, decomposing contaminants in spacecrafts and decomposition of solid propellants, battery anodes, and radiation shielding are most inviting. Among the available materials, stannic dioxide nanoparticles stand with wide band gap of about 3.6 eV, sensitive electrical conductance, photocatalytic action, reliability in low pressure and vacuum, light weight, and capable of detecting trace gases at ppm levels. Rightly, it is studied for sensing carbon monoxide and hydrogen in ISS environmental control systems and planetary rover instruments.

The electrical conductance of stannic dioxide nanoparticles is sensitive to exposure of CO, CO_2, O_2, CH_4, H_2, NH_3, etc. It can be applied for sensors to monitor the atmosphere of extraterrestrial habitat, and air quality inside spacecrafts. The large surface-to-volume ratio imparts it high sensitivity and high speed of response [1]. It can be incorporated in planetary exploration instruments, planetary landers or rovers, and volcanic or cryogenic plume analyzers.

Its transparency and conductivity make it suited for electron transport layers required in dye-sensitized and perovskite solar cells of spacecrafts. Lithium-ion batteries use it as anode materials due its high capacity. It is suited for energy storage in satellites [2].

The photocatalytic activity in ultraviolet range imparts stannic dioxide np a capacity to decompose organic contaminants of spacecraft. The surfaces of satellites, spacecrafts and telescopes accumulate hydrocarbons in orbits which can be self-cleaned by the SnO_2-NP. Its wide band gap and high stability under radiation make it more suited for the work [3-5]. It can be important combustion enhancing and hydrazine decomposer used in spacecraft thrusters.

SnO_2-NP doped with heavy metals can be used develop good radiation absorbers. Its thin films will act as radiation shields of electronic equipment exposed to cosmic radiation in orbits.

The challenge lies in synthesis of suitable nanophase stannic dioxide. It can be synthesized by various methods such as spray pyrolysis or flame spray synthesis [6, 7], laser removal process [8], mini arc plasma [9], hydrothermal [10, 11], amorphous citrate route [12], wet chemical method [13], solid-state reaction [14], sol-gel [15, 16], co-precipitation [17], and so on.

We prepared pure stannic oxide nanomaterial samples by eco-friendly facile co-precipitation method. As prepared sample was characterized by x-ray diffraction for crystal structure, crystallite size and microstrain, by SEM for morphology and by DLS-zeta potential for stability. Its UV-visible spectroscopy and vibrating sample magnetometry indicated, respectively, a blue shifted band gap and ferromagnetic phase hysteresis loop.

2. Experimental Method

The chemicals of analytic grade, $SnCl_4.5H_2O$ (98%purity, Sigma Aldrich) and aqueous ammonia (25 w/w, Rankem), were procured and used without further purification. To prepare a pristine sample of SnO_2, first a solution was prepared by dissolving its 3.510 g in 100ml de-ionized water at room temperature. Then it was put on a hot plate with magnetic stirrer and heated to 35°C. Now, aqueous Ammonia was added to it drop-by-drop with stirring until the white precipitate was obtained (pH value of 8). After 35 minutes of stirring, the solution was filtered to get the precipitate. The precipitate was rinsed several times with de-ionized water. The washed precipitate was dried at 120°C for 4.50 hours. It was then left for natural cooling to room temperature. Finally,

the sample in powder form was collected for characterizations.

3. Results and Discussion

The powder sample was put to an x-ray diffraction experiment in machine RIGAKU MINI FLEX 600, using copper-K-alpha radiation of wavelength 1.5406 angstroms. The scan rate used was 2 degrees per minute in steps of 0.02 degrees from 20 to 80 degrees span. These patterns appear in Figures 1. The broadening of peaks is indicative of small particles in the sample.

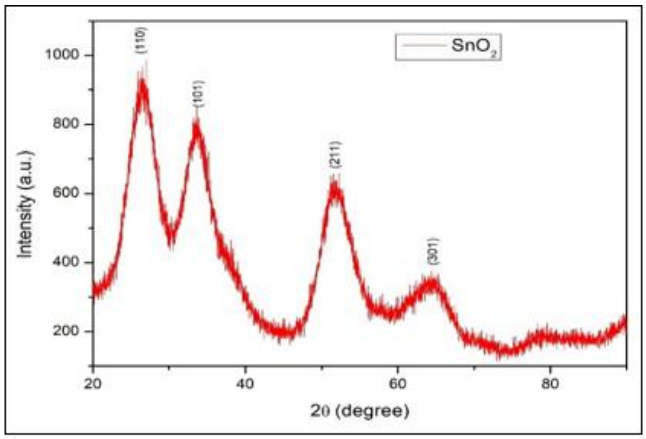

Figure 1: X-ray diffraction pattern of pristine SnO_2 nanoparticles

Lattice spacings a and c of the tetragonal unit cell of stannic dioxide were calculated using the Miller indices. The peak positions are related to Bragg spacing d as

$$2d_{hkl} \sin \theta_{hkl} = \lambda \qquad (1)$$

The lattice parameters of a tetragonal unit cell are given by

$$\frac{1}{d_{hkl}^2} = \frac{h^2 + k^2}{a^2} + \frac{l^2}{c^2} \qquad (2)$$

Using the position and Miller indices of (110) peak in equations (1) and (2), we get

$$a = \frac{0.707\ \lambda}{\sin \theta_{110}}$$

With this a, and position of the peak at (101), we get c. The observed values are $a = b = 4.75$ Å and c= 3.22 Å .

Crystalline parameters are consistent with JCPDS file 41-1445.

Table 1: Peak positions and lattice parameters

$2\theta_{hkl}$(Degree)	Miller Indices	Lattice parameters
26.530	110	$a=b$=4.75 Å c=3.22 Å
33.609	101	
51.981	211	
63.737	301	

The crystallite size was obtained from the x-ray diffractogram using Williamson-Hall plot. The full width at half the maximum (FWHM) β and half-angular positions of peaks θ were measured and used in plotting equation (3). The net broadening is given by Williamson and Hall equation for all the peaks as

$$\beta_{hkl} \cos \theta_{hkl} = \frac{k\lambda}{D} + \epsilon\ (4 \sin \theta_{hkl}) \qquad (3)$$

Data Table 2 shows the FWHM of all the intense peaks. These are employed to scatter plot the data and get a linear fit (Figure 2) WH plot.

Table 2: WH Plot for microstrain and grain size.

Peak Miller indices	FWHM (Degree)	$(4\sin\theta_{hkl})$	$\beta_{hkl}\cos\theta_{hkl}$	Microstrain	Grain size, nm
110	3.584	0.91782	0.06087	0.012	3.13
101	3.345	1.15643	0.05588		
211	4.404	1.175289	0.06912		
301	10.968	Masked point	Masked point		

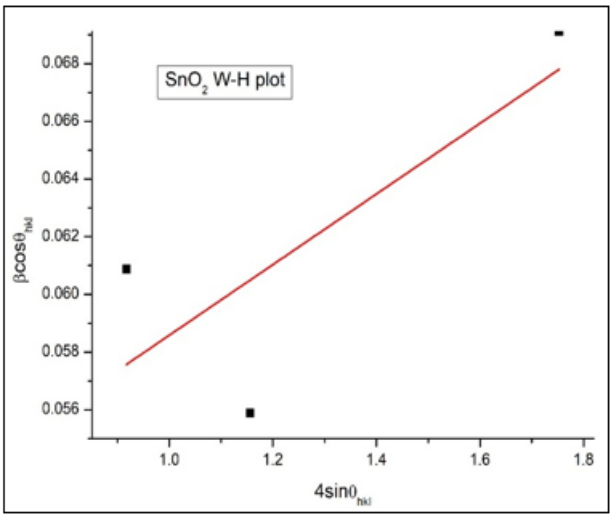

Figure 2: WH plot of pristine SnO_2 nanoparticles

The slope of the straight line gives a microstrain of 0.012. The intercept on the ordinate-axis was measured and mean size of particles were observed as 3.13 nm.

Figure 3 shows SEM image of the prepared sample. SEM image shows fine agglomerated particles.

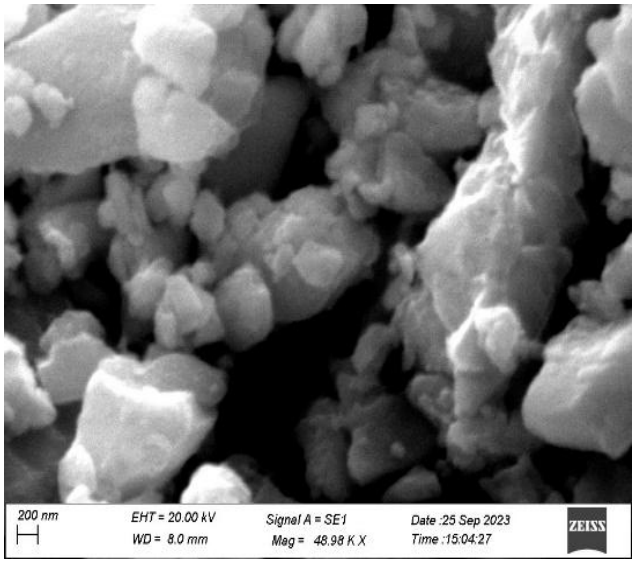

Figure 3: SEM image of SnO_2

For spheres, surface-to-volume ratio is inversely proportional to radius. The smaller the sphere, the larger the ratio. Nanoparticles are such materials, and show high reactivity, absorptivity, and electrical super capacity.

Zeta potential measurement for stability

The impression of SEM image was correlated to zeta potential measurement. Agglomeration of particles under van der Waals interactions is an important aspect of nanoparticles either in solutions or in suspension. Electrostatic charge on particle surfaces is, therefore, studied in a dispersive medium. To prevent such effect, the significant factors are pH, ionic concentration, viscosity, and dielectric constant. A charged nanoparticle attracts opposite charges in the liquid medium around it, which adhere to it and move with it in the medium. This layer is called stern layer. There forms a second layer on it whose end slips on liquid. A double layer is thus formed on the nanoparticle. Beyond the double layer, electroneutral medium exists. Diffuse layer is union of layers after the stern layer.

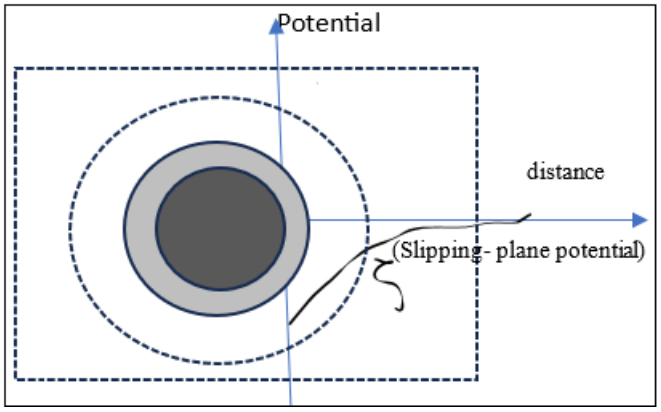

Figure 4: The nanoparticle and layers: zeta potential

As in Figure 4, the charge on the nanoparticle may be negative, and the surface potential, stern potential, and the potential at slipping plane in the double layer are all negative with respect to the far away electroneutral region. Two nanoparticles having like charges of enough magnitude strongly repel each other so as to win over the attractive van der Waals forces. To measure zeta potential an electric field is applied on the nanoparticle in the medium. The resulting velocity is measured using dynamic light scattering (DLS)apparatus. The zeta potential is calculated using an equation, called Smoluchowski equation or Henry equation in terms of mobility μ, particle radius R, ionic strength I, temperature T, dielectric constant ϵ, and viscosity coefficient η. The zeta potential is given by

$$\zeta = \frac{3\eta\mu}{2\epsilon_0\epsilon\, f(\kappa R)}$$

The Henry's function, $f(\kappa R)$ in the Smoluchowski limit, is 1.5. Then, zeta potential is

$$\zeta = \frac{\eta\mu}{\epsilon_0\epsilon}$$

It is observed that $-10\,mV \leq \zeta \leq 10mV$, strong agglomeration occurs, while for about $|\zeta| \geq 25\,mV$, well dispersed stable particles are obtained. For stannic dioxide nanoparticles, zeta potential was measured using NANOPLUS Common, version 5.22/3.00. The plot in Figure 5 indicates the range of zeta potential from -34 mV to 17.6 mV.

The high magnitude negative values in the plot (Figure 5) show stability while the positive value of 17 mV is less than enough, and suggests agglomeration. SEM image can be tagged to this result.

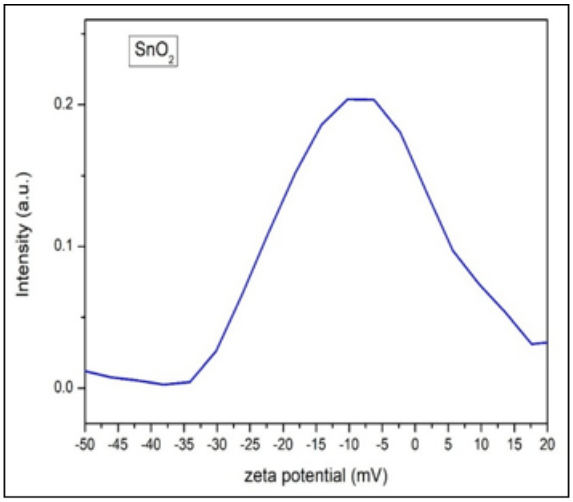

Figure 5: Zeta potential plot of stannic dioxide sample

Band gap measurement

The behaviour of materials in outer space must be checked against ultraviolet and visible radiations. Especially, band gap is an important determiner of photocatalytic and energy applications. Absorption was observed in ultraviolet region giving a band gap of 4.39 eV which is blue shifted relative to the bulk value of 3.6 eV. Tauc's plot (Figure 6) is a graphical solution of the equation for direct band gap semiconductor SnO_2

$$(h\nu\alpha)^2 = B\,(h\nu - Eo)$$

The straight line of RHS and curve of LHS satisfy a region of graph, and upon extension of straight line to the energy-axis, it cuts in $h\nu = Eo$, the band gap. The observed band gap is 4.39 eV which is blue shifted relative to bulk value of 3.6 eV.

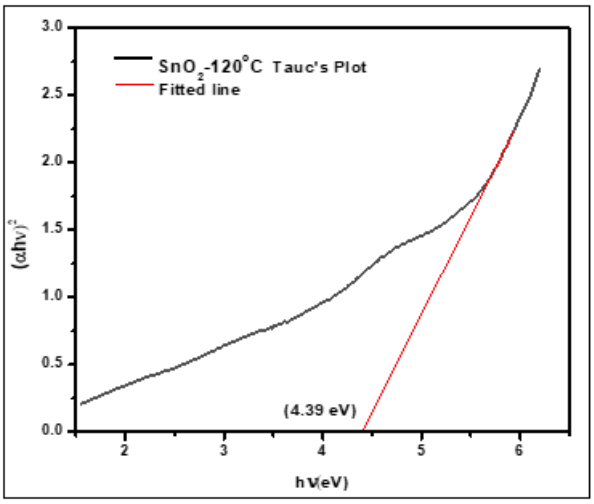

Figure 6: Band Gap Measurement from UV-VIS absorption

Magnetic measurement: defect induced FM

The sample was exposed to magnetic field of vibrating sample magnetometer (VSM), and magnetization data against applied magnetic field intensity H, were acquired. The plot of M against H is as shown in Figure 7. The M-H curve shows a hysteretic loop, observed in FM. However, the

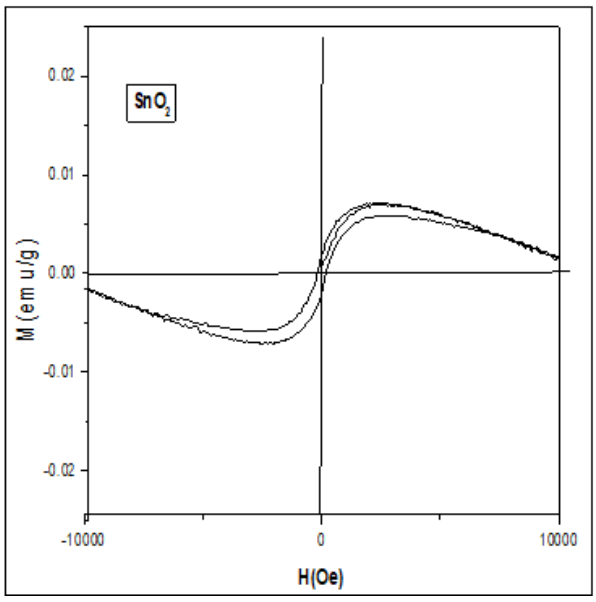

Figure 7: Hysteresis loop of ferromagnetic behaviour

magnetization slowly decreases by increasing field H, and saturation is not sharp. This is not an experimental error, rather it is natural for such oxides with oxygen and interstitial defects. As the field H increases, two factors start contributing moments in proportion or so to H: slowly rising paramagnetic and opposite dominating diamagnetic moments. A small source may be fall in FM strength due to delocalization of trapped electrons at high fields, shrinking of polaron regions, weakening of exchange interactions, and high field spin canting Thus, net magnetization falls gradually by increasing H. The ferromagnetism observed is 'defect induced'.

4. Conclusion

Nanophase stannic dioxide was prepared successfully for its applications by a green chemical method. XRD patterns suggested crystalline phase of tetragonal unit cell having lattice parameters consistent with JCPDS data file 41-1445. SEM and zeta potential analysis exhibited agglomerated samples, while WH plots gave a particle size near 3 nm and strain of 0.0012. The band gap of 4.39 eV showed blue shift due to quantum confinement, and a ferromagnetism in undoped SnO_2 possibly due to defect states. Magnetization exhibited diamagnetic quenching at higher fields. It suits its applications in space.

Acknowledgement

Authors are grateful to Institutions for using their physical laboratories, and to the Departments for academic supports to the research work.

References

[1] Masuda, Y, 'Recent advances in SnO_2 nanostructure-based gas sensors', *ScienceDirect*, (2022).
[2] Xie H, et al, 'Solvothermal synthesis of SnO2 nanoparticles .., *Frontier in Chemistry*, (2024)
[3] W. Pi et al, 'The gas sensing performance of a core shell SnO2 based chemiesistive MEMS sensor for H2S detection under vacuum'*Journal of Materials Chemistry C* (2023)
[4] *NASA* Glenn, 'Chemical Sensors'
[5] G.B. Nam, 'Real-time Tunable Gas sensing platform based on SnO_2., *SpringerLink* (2024)
[6] Liu W and H Wang, *Journal of Materiomics*, **6**, 385-96(2020)
[7] T Sahm, L Madler, A Gurlo, N Barsan, S E Pratsinis, and U. Weimar, *Sens. Actuators B*, **81,**165-169 (2004)
[8] F Paraguay-Delgado, W Antunez-Flores, M Miki-Yoshida, A Anguilar- Elguezabal,P Santiago, R Diaz and J A Ascencio, *Nanotechnology*,**16** 688 (2005).
[9] G Lu, K L Huebner, L E Ocola, M G Josifovska, and J Chen, *J. Nanomaterials*, 1-7(2006)
[10] S Fujihara, T. Maeda, H Ohgi, E Hosono, H. Imai, and S H Kim, *A Chem. Society*, **20**, 6476-6481(2004)
[11] F Shaikh et al, *Powder Technol*. **326**, 479-87 (2018)
[12] M Bhagwat, P. Shah, V. Ramaswamy, *Materials Letters*.**57**, 1604-1611(2003)
[13] S Gnanam and V Rajendran, *Digest Journal of Nanomaterials and Biostructures*, **5,** 699-704(2010)
[14] F. Li, J. Xu, X. Yu, L Chen, J. Zhu, Z. Yang and X. Xin, *Sens. Actuators B***, 81**, 165-169 (2002)
[15] L.L. Hench and J K West, *Chem. Rev.,* **90**, 33-72(1990)
[16] L P Wang et al, *Adv. Mater*. **29**, 1603286 (2017)
[17] G. Lu et al, *Sens. Actuators B: Chemical* **162**, 82-8(2012)